

Review Article: FePt heat assisted magnetic recording media

Dieter Weller, Gregory Parker, Oleksandr Mosendz, Andreas Lyberatos, Dmitriy Mitin, Nataliia Y. Safonova, and Manfred Albrecht

Citation: *Journal of Vacuum Science & Technology B, Nanotechnology and Microelectronics: Materials, Processing, Measurement, and Phenomena* **34**, 060801 (2016); doi: 10.1116/1.4965980

View online: <https://doi.org/10.1116/1.4965980>

View Table of Contents: <http://avs.scitation.org/toc/jvb/34/6>

Published by the [American Vacuum Society](#)

Articles you may be interested in

[Heat-assisted magnetic recording of bit-patterned media beyond 10 Tb/in²](#)
Applied Physics Letters **108**, 102406 (2016); 10.1063/1.4943629

[MgO-C interlayer for grain size control in FePt-C media for heat assisted magnetic recording](#)
AIP Advances **7**, 056503 (2017); 10.1063/1.4973500

[Thermal switching probability distribution of L10 FePt for heat assisted magnetic recording](#)
Applied Physics Letters **110**, 182405 (2017); 10.1063/1.4983033

[The Curie temperature distribution of FePt granular magnetic recording media](#)
Applied Physics Letters **101**, 052406 (2012); 10.1063/1.4740075

[Growth of L1₀-ordered crystal in FePt and FePd thin films on MgO\(001\) substrate](#)
AIP Advances **6**, 085302 (2016); 10.1063/1.4960554

[FeRh/FePt exchange spring films for thermally assisted magnetic recording media](#)
Applied Physics Letters **82**, 2859 (2003); 10.1063/1.1571232



Instruments for Advanced Science

Contact Hiden Analytical for further details:
W www.HidenAnalytical.com
E info@hiden.co.uk

CLICK TO VIEW our product catalogue



Gas Analysis

- dynamic measurement of reaction gas streams
- catalysis and thermal analysis
- molecular beam studies
- dissolved species probes
- fermentation, environmental and ecological studies



Surface Science

- UHV TPD
- SIMS
- end point detection in ion beam etch
- elemental imaging - surface mapping



Plasma Diagnostics

- plasma source characterization
- etch and deposition process reaction kinetic studies
- analysis of neutral and radical species



Vacuum Analysis

- partial pressure measurement and control of process gases
- reactive sputter process control
- vacuum diagnostics
- vacuum coating process monitoring

Review Article: FePt heat assisted magnetic recording media

Dieter Weller^{a)}

HGST, a Western Digital Company, San Jose Research Center, San Jose, California 95135 and Institute of Physics, University of Augsburg, D-86159 Augsburg, Germany

Gregory Parker and Oleksandr Mosendz

HGST, a Western Digital Company, San Jose Research Center, San Jose, California 95135

Andreas Lyberatos

Department of Materials Science and Technology, University of Crete, Heraklion 71003, Greece

Dmitriy Mitin, Nataliia Y. Safonova, and Manfred Albrecht

Institute of Physics, University of Augsburg, D-86159 Augsburg, Germany

(Received 9 September 2016; accepted 29 September 2016; published 26 October 2016)

Heat-assisted magnetic recording (HAMR) media status, requirements, and challenges to extend the areal density (AD) of magnetic hard disk drives beyond current records of around 1.4 Tb/in.² are updated. The structural properties of granular high anisotropy chemically ordered L1₀ FePtX-Y HAMR media by now are similar to perpendicular CoCrPt-based magnetic recording media. Reasonable average grain diameter $\langle D \rangle = 8\text{--}10$ nm and distributions $\sigma_D/D \sim 18\%$ are possible despite elevated growth temperatures $T_G = 650\text{--}670$ °C. A $2\times$ reduction of $\langle D \rangle$ down to 4–5 nm and lowering $\sigma_D/D < 10\%\text{--}15\%$ are ongoing efforts to increase AD to ~ 4 Tb/in.². X = Cu ~ 10 at. % reduces the Curie temperature T_C by ~ 100 K below $T_{C,\text{bulk}} = 750$ K, thereby lowering the write head heat energy requirement. Multiple FePtX-Y granular layers with Y = 30–35 vol. % grain-to-grain segregants like carbides, oxides, and/or nitrides are used to fully exchange decouple the grains and achieve cylindrical shape. FePt is typically grown on fcc MgO (100) seedlayers to form well oriented FePt (002). A FePt lattice parameter ratio $c/a \sim 0.96$ and high chemical order $S > 0.90$ result in magnetic anisotropy $K_U \sim 4.5 \times 10^7$ erg/cm³, and only 25% below the FePt single crystal value $K_U = 6.6 \times 10^7$ erg/cm³ has been achieved in 7–8 nm diameter grains. Switching field distributions depend on anisotropy field (H_K) distributions, which are currently of the order of $\Delta H_K/H_K \sim 10\%$ ($\Delta H_K \sim 10\text{--}12$ kOe, $H_K \sim 10\text{--}11$ T) at room temperature. High thermal conductivity heat sink layers, including Ag, Au, Cu, and Cr, are used to optimize the cooling rate and maximize the down- and cross-track thermal gradient, which determines the achievable track density. © 2016 Author(s). All article content, except where otherwise noted, is licensed under a Creative Commons Attribution (CC BY) license (<http://creativecommons.org/licenses/by/4.0/>). [<http://dx.doi.org/10.1116/1.4965980>]

I. INTRODUCTION

Heat-assisted magnetic recording (HAMR) is a new magnetic hard disk drive (HDD) technology, which is expected to extend the 1 Tb/in.² areal density (AD) demonstrated by perpendicular magnetic recording (PMR) toward 3–4 Tb/in.². AD is determined by magnetic flux changes in the linear down-track direction (fci = flux changes per inch) multiplied by cross track density (tpi = tracks per inch). In today's mobile PMR products AD is ~ 1200 Gb/in.² with a bit aspect ratio (BAR) ~ 4 . The highest areal density PMR media have about 6–10 grains per bit with an average diameter $\langle D \rangle \sim 8$ nm. Future HAMR media based on chemically ordered L1₀ FePt (002) with 5–10 \times higher magnetic anisotropy $K_U \sim 4.5 \times 10^7$ erg/cc allow smaller thermally stable grains ultimately down to $\langle D \rangle \sim 4$ nm.^{1–5} In order to write bits into such media, a laser combined with a near field transducer (NFT) locally heats the

medium above the Curie temperature T_C , followed by rapid thermal cooling in the presence of the head field. Seagate has demonstrated HAMR recording with $AD = 1.4$ Tb/in.² and $BAR \sim 3$.^{3–5} Average grain size $\langle D \rangle \sim 9$ nm and grain center-to-center spacing (pitch) ~ 10.5 nm were reported.³ The experimental bit-error-rate (BER), which depends on the signal-to-noise-ratio (SNR), was $\sim 10^{-2}$, which nowadays is sufficient based on error correction methods in signal channels.^{6,7}

The read-back signal depends on the remanent magnetization (M_R), the magnetic layer thickness (δ), and the read head-disk spacing. The media noise is dominated by transition position fluctuations (jitter), which strongly depend on the number of grains per bit and their physical as well as cluster size distributions. In addition, there is some randomness in grain locations, texture variation, crystallographic orientation variation (c-axis angle fluctuations), and magnetic nonuniformity.^{8,9}

Figure 1 shows the combination of HAMR head and media, highlighting the so-called NFT,¹⁰ head-disk interface,

^{a)}Electronic mail: dtrweller@gmail.com

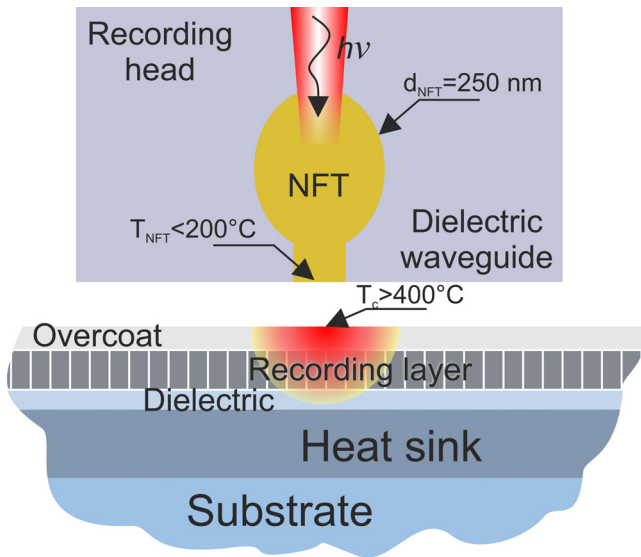


FIG. 1. (Color online) HAMR head and media including key spacing and thickness parameters.

and key HAMR media layers, including a substrate, heat sink, dielectric or seed layer, the granular FePt recording layer, as well as a C-based overcoat layer.¹¹ Some key dimensions are included.

Similar to the magnetic image charge created by a soft underlayer used in PMR, the heatsink layer used to control the heat flow in the HAMR media can also be used to generate an electronic image charge if plasmonic materials, such as Au are used for the heatsink. Plasmons are excited in the heatsink by photons from the NFT, increasing the coupling efficiency and decreasing the overall power requirement of the system.²⁻⁵

Figure 2 is an illustration of HAMR head and media, including the heated spot (a) and the temperature dependent FePt media coercivity during heating and cooling (b).¹² It shows the narrow hot spot on the media, which during recording determines the bit transition and track width. Heating above the Curie temperature is needed, and recording occurs during rapid cooling on the trailing edge of the temperature profile.²

II. HAMR MEDIA OVERVIEW

Key HAMR media requirements have been summarized and discussed, e.g., by Rottmayer *et al.*¹³ and Granz and Kryder.¹⁴ A recent review book article by Hono *et al.*¹⁵

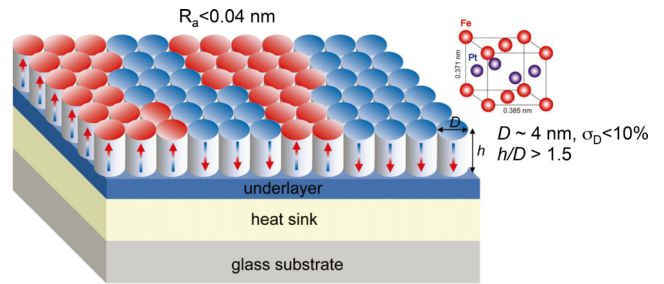


FIG. 3. (Color online) Ideal structure of a HAMR medium at 4 Tbit/in² areal density. Light and dark colors show the direction of magnetic poles. The L1₀-FePt crystal (upper-right figure) must grow cylindrical columns separated by nonmagnetic segregants (Ref. 15). [Reprinted with permission from Hono *et al.*, *Ultra-High-Density Magnetic Recording, Storage Materials and Media Designs* edited by G. Varvaro and F. Casoli (Pan Stanford, 2016), Chap. 5, pp. 245–277. Copyright 2016, Pan Stanford.]

summarizes granular HAMR media data. The required recording (heating) temperature is above the local T_C , which strongly depends on the grain size and chemical ordering as demonstrated in experiments^{16,17} and modeling.¹⁸⁻²⁰ T_C reduction when lowering the grain size is consistent with a finite-size scaling theory.¹⁹ An optimum thickness-diameter ratio of $\delta/D = 1.5-2.5$ is suggested to “avoid” T_C variation.^{19,20} The fact that bulk $T_C = 585$ K of disordered fcc Al FePt is much lower than $T_C = 750$ K of fully chemically ordered fct L1₀ FePt (Refs. 21 and 22) correlates magnetic distributions with T_C distributions due to grain size and shape dependence of chemical ordering.

Monte Carlo calculations by Lyberatos *et al.*^{18,19} have shown that at an aspect ratio $\delta/D \sim 2$, the finite size effects on T_C are minimized. These modeling results were limited to FePt grains of rather small diameter $D = 3$ nm, since for larger grains, the error rate due to critical slowing down is large. The optimal aspect ratio is not expected to depend on the choice of the in-plane grain diameter D , according to finite size scaling theory.

Figure 3 illustrates an ideal structure of future HAMR media with an areal density potential of 4 Tbit/in.²^{15,23} Key layers include proper heat sink and FePt seed or underlayers on glass substrates. The goal is to achieve cylindrical grains or columns with a diameter down to $D \sim 4$ nm, a grain diameter variation $\sigma_D < 10\%$, and a thickness-diameter ratio $\delta/D > 1.5$. Details are discussed in Sec. III A.

Key experimental findings are that highly chemically ordered granular L1₀ FePtX-Y media can be sputter-deposited on suitable, high rigidity glass substrates at temperatures up to

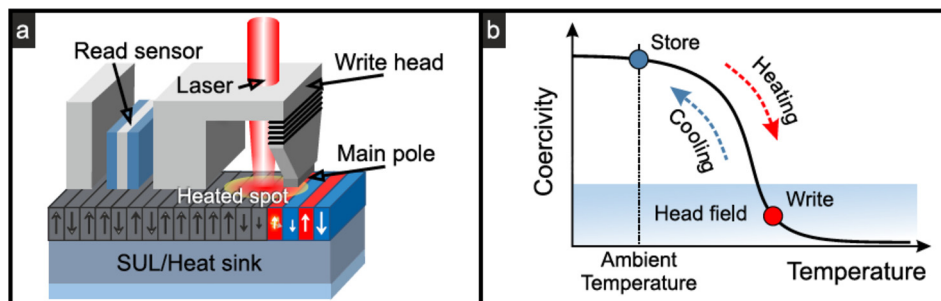


FIG. 2. (Color online) (a) Typical HAMR head-media recording image and (b) temperature dependent FePt media coercivity.

650–670 °C. They are promising candidates for future HAMR products.^{2–5,13–15} Hono *et al.*,¹⁵ Granz and Kryder,¹⁴ and Weller *et al.*² recently reviewed compositions and grain segregants, based on x-ray diffraction (XRD) and transmission electron microscopy (TEM) experiments. The presence and degree of L1₀ ordering is characterized by XRD. The FePt(002) diffraction peak is well defined and indicates a high degree of texture. The superlattice FePt(001) peak and the intensity ratio $A(001)/A(002) \sim 2$ indicate proper chemical ordering $S \sim 0.45 \times [A(001)/A(002)]^{1/2} = 0.9$ in current media. The ultimate goal for optimized media is of course 100% chemical ordering, which down the road will reduce the read-back noise and accordingly will improve SNR. Misorientation of the easy axes and random texturing of grains can be suppressed by optimizing the deposition parameters, such as Ar pressure, power, base pressure, growth rate, segregant choice, and amount.^{2,15} Mosendz *et al.*²⁴ reported an average grain size diameter of $\langle D \rangle = 7.2$ nm and a size distribution of $\sigma_D/\langle D \rangle = 16\%$ with $X = \text{Ag}$ (10 at. %) and $Y = \text{C}$ (35 vol. %) in “early” FePtAg-C media. Using carbon segregants in these single layer media resulted in spherically shaped grains, which roughly limits the thickness-to-grain diameter ratio to $\delta/D \sim 0.8\text{--}1.0$.^{24,25}

Moving from single to dual, triple, quadruple, or even higher multiple “layer” granular media with different segregants, compositions, and growth conditions for each step is used to optimize HAMR media. A specific example is FePt-C/FePt-SiO₂ or TiO₂.²⁷ Improvements include modification of the grain shape from spherical to cylindrical and increased experimental thickness–diameter ratio δ/D from <1 to about 1.5.^{2,15,26}

Coercivities up to $H_C \sim 5.2$ T, anisotropy fields $H_K > 9$ T, and perpendicular magnetic anisotropy energy densities $K_u \sim 4.5 \times 10^7$ erg/cm³ (Refs. 2, 15, and 26) can be achieved in such media structures. Measurements with high field $H \sim 14$ T in physical property measurement system (PPMS) vibrating sample magnetometer (VSM) tools reveal typical values $H_K \sim 10\text{--}11$ T.^{28,29} Recent ferromagnetic resonance measurements interestingly also indicate a relatively high damping parameter $\alpha \sim 0.1$ in single layer FePtAg-C granular alloys.²⁹

Models to better understand signal and noise dependences in HAMR are discussed by Zhu and Li³⁰ and Victora and Huang.³¹ A lot of focus is on doping FePtX with $X = \text{Cu}$ to tune the magnetic anisotropy and adjust (lower) the Curie temperature in order to reduce laser power requirements^{2,15,32–41} as well as optimizing relevant HAMR media measurements.⁴² A typical example is a 100 K T_C reduction with about 10 at. % Cu.^{2,15} Another proposed and interesting recording topic is laser pulsing instead of constant laser heating on rotating disks, which may help to increase SNR, as discussed by Richter *et al.*⁴³

Another important area for future HAMR media is more complex coupled structures like composite-granular-continuous⁴⁴ and exchange-coupled-composite type media.^{45–48} The potential of tailoring media for HAMR by changing the temperature response of the material properties was recognized early on in a study of Ni-doped FePt films⁴⁹ and studies of more ECC-like media structures using multiple layers

with different temperature dependencies, such as bilayers of FePt and FeRh,⁵⁰ or soft Fe coupled to FePt.⁴⁷ The ECC concept has successfully been adapted for use in today’s PMR media. Recently, the magnetic reversal behavior in hard/soft bilayer thin-films with 90° coupling angle has been discussed.⁵¹ Furthermore, heat assisted magnetic recording composite media, consisting of a superparamagnetic writing layer and a (doped) FePt storage layer, were proposed.⁵² The advantages include reduced sensitivity to T_C variance in the storage layer, and the opportunity to significantly lower the T_C of the FePt storage layer without increasing the T_C distributions, which adversely affect the recording performance.

Initially, the concept of ECC media was suggested to reduce the switching field of a hard magnetic layer.^{53,54} A grain of such a medium consists of a soft part in which the reversal nucleates and a hard part, which provides thermal stability. These systems switch by nucleation and domain wall motion. As a soft magnetic layer, Fe is a commonly employed material, because of its small magnetocrystalline anisotropy and large saturation magnetization.^{54–61} Different bilayer stacks as well as more complex ECC structures like trilayers⁶² were proposed, and their magnetic properties dependent on the soft layer thickness were investigated,^{63–65} demonstrating the superior performance of ECC media.

Furthermore, Suess and Schrefl⁶⁶ proposed an elegant way by using ECC bilayers having different Curie temperatures to overcome the current limitation in HAMR recording density of about 20 Tb/in.^{2,67} This limit, which is given by thermally induced recording errors, can be lifted by introducing a composite structure of two exchange coupled materials. In this case, the storage material at the bottom has a Curie temperature close to the write temperature T_{wr} , and the other material on top has a significantly higher T_C . It was calculated that for a FePt/Fe ECC bilayer an areal density up to 54 Tb/in.² can be achieved.

III. SPUTTERED HAMR MEDIA

Magnetron sputtering is used to generate fiber-textured FePt HAMR media with small grains and high magnetocrystalline anisotropy. The crystalline orientation is controlled by epitaxial growth on MgO (001) seed layers. Proper combination of composition, segregants, deposition parameters, and deposition temperature is used to optimize the properties of granular FePt films. Key challenges in HAMR media fabrication include the reduction of grain diameter, size distribution, as well as control of microstructure and magnetic properties. Progress, including media design and recording modeling, is reviewed in Ref. 2. Highlights and details are discussed in the following.

A. FePt media design, texture and chemical ordering review

A typical simplistic “FePt media design” consists of “high T glass substrate/20–100 nm amorphous a-NiTa/20–200 nm thermal conductivity heatsink layer/5–20 nm MgO seedlayer/heating to 650 °C/6–12 nm FePtX-Y/cooling to <100 °C/COC/high T lube.” High temperature glass

substrates are available from different companies, e.g., Hoya,⁷⁰ Ohara,⁷¹ and Asahi,⁷² which currently allows growth and/or annealing up to 650–670 °C without surface distortion or bending. Elevated growth temperatures are needed to allow improvements in chemical ordering of the FePt layer toward 100%. In general, the choice, combination, and thicknesses of seed and heat sink layers are critical to improve and optimize FePt growth conditions and thermal properties. Various options of choice and growth optimizations of these layers have been tried and discussed since the early 1990s to develop and improve granular L1₀ FePt media.^{2–5,10,11,19–27}

Figure 3 shows the general HAMR media design structure.^{2–5,13–15} Glass disk substrates are coated with a smooth amorphous adhesion layer like 20–100 nm thick amorphous NiTa, which does not affect the magnetic materials deposited thereon. This is followed by an approximately 50 nm thick high thermal heat-dissipating (heat sink) layer, which, depending on the NFT design, may also act as a plasmonic underlayer when illuminated during HAMR recording. Examples include Ag, Al, Cu, Cr, Au, and NiAl with thermal conductivity >30 W/mK. The heat sink layer is configured to allow heat deposited in the magnetic recording layer to quickly dissipate and limit lateral heat flow in FePt.

On top of the heat sink layer a 5–15 nm relatively thin [002] textured fcc MgO layer is deposited. This is very relevant and important for proper (001) orientation of FePt. Several alternatives to MgO include CrRu, CrMo, TiN, and TiC.^{2–5,11} Recently, high electrical conductivity (Mg_{0.2}Ti_{0.8})O (MTO) seedlayers with a strong [002] texture and better wettability have been studied.⁷³ MTO also helps adhesion and improves chemical stability over time, which may be a problem when using MgO. Based on a number of recent studies of FePt(001) growth on single crystalline epitaxial (La,Sr)(Al,Ta)O₃, SrTiO₃, and MgAl₂O₄ seed layers, where the a-axis lattice mismatch with FePt (001) is varied relative to single crystalline MgO,⁹ it can be concluded that the large lateral a-parameter expansion or lattice misfit strain of ~9% at the FePt(001)/MgO(001) interface is very relevant and important to achieve proper [001] perpendicular c-axis orientation and the ultimate c/a ~ 0.96 ratio of fully chemically ordered L1₀ FePt(001).^{2–5,9,15}

Note that polycrystalline fractions of sputtered MgO seedlayers introduce significant misorientations in the (002)-textured FePt grains, which cause easy axis (EA) distributions of >3%, as highlighted by Wang *et al.*⁴²

While all seed- and heat sink layers can be sputtered at temperatures slightly above room temperature, the growth of FePt requires elevated temperatures close to the maximum temperature of ~670 °C that glass substrates “survive” without bending or distortion.

To achieve the required granularity for magnetic recording applications, FePt is cosputtered with segregants or magnetic isolators to ultimately achieve granular close to cylindrical FePt hard permanent magnet grains or nanoparticles. Proper segregants promote structural and magnetic grain isolation to each other and define the grain shape. They include carbon, carbides, oxides and/or nitrides. Specific examples are SiO₂, SiN_x, B₂O₃,^{2,11,25,74} BN,⁷⁵ and Cr₂O₃.⁷⁶

Another interesting and relevant topic is FePtX with X ~ 10 at. % Ag, which reduces the required growth temperature to achieve high chemically ordered L1₀ FePt. Mosendz *et al.*²⁴ have discussed granular Fe₄₅Pt₄₅Ag₁₀-C media fabrication where ~10 at. % Ag allows ~50 K reduction in the deposition temperature to achieve higher chemical L1₀ FePt ordering. A sputtered 6 nm thick FePtAg-C (35 at. %) film produces spherical magnetic grains and a bimodal distribution of magnetic grain sizes.²⁴ Zhang *et al.*⁷⁷ and Varaprasad *et al.*⁷⁸ highlight coercivity enhancements when using Ag ~ 10 at. % in FePtAg-C granular films. What is also very beneficial is that Ag segregates to the edges of grains and in principal does not impact the FePt grain magnetic properties.¹⁵

Dual, triple, quadruple, or higher order lamination layers were first reported by Varaprasad *et al.* in 2013 (Ref. 27) and are highlighted by Hellwig *et al.*⁷⁹ in a recent patent, which includes very detailed descriptions of HAMR media designs and selected materials. An early example is dual FePt-C (6 nm)/FePt-TiO₂ (2 nm) bilayers, showing a columnar structure due to the thin FePt-TiO₂ layer on top. In the perpendicular magnetization curve, however, there is reduced remanence at zero magnetic field, due to the soft magnetic feature of the FePt-TiO₂ layer.

B. FeCuPt/Fe ECC media

A recent example of an ECC layer stack, consisting of a FeCuPt/Fe bilayer, is presented in the following. Bilayers of FePt/Cu were dc magnetron sputter-deposited at room temperature on Si(100) substrates with a 100 nm thick thermally oxidized amorphous SiO₂ layer. After deposition, the samples were processed by rapid thermal annealing (RTA) at 700 °C for 30 s in N₂ atmosphere. It has been demonstrated that RTA processing of FePt/Cu bilayers does not only lead to chemical ordering but also to the development of a (001) texture on amorphous substrates,^{41–56,68} which reveals the high potential of an RTA process for the fabrication of future FePt-based devices.

All FeCuPt films exhibit an out-of-plane easy axis magnetization and a strong reduction of the out-of-plane coercivity and saturation magnetization with increasing Cu content [Fig. 4(a)]. At the same time, the perpendicular magnetic anisotropy K_u drops from 1.2×10^7 to 0.8×10^7 erg/cm³ [Fig. 4(b)]. The temperature dependence of the magnetization (M - T curve) was measured by superconducting quantum interference device (SQUID)-VSM up to 600 °C in in-plane geometry under an applied in-plane field of 500 Oe. As shown in Fig. 4(c), the addition of Cu leads to a Curie temperature reduction from 400 to 320 °C for the FeCuPt film with the highest Cu content.

Two hard magnetic FeCuPt films with 3 and 10 at. % of Cu were selected for the next deposition step, where Fe layers of various thicknesses between 1 and 4 nm were deposited at room temperature. For Fe layers thinner than the Fe exchange length l_{ex} of about 2 nm,⁶⁹ strong exchange coupling between Fe and FeCuPt results in an out-of-plane magnetization orientation of the bilayer. By contrast, bilayers with thicker Fe layers reveal an in-plane magnetic anisotropy of the Fe layer. As summarized in Fig. 4(d), a

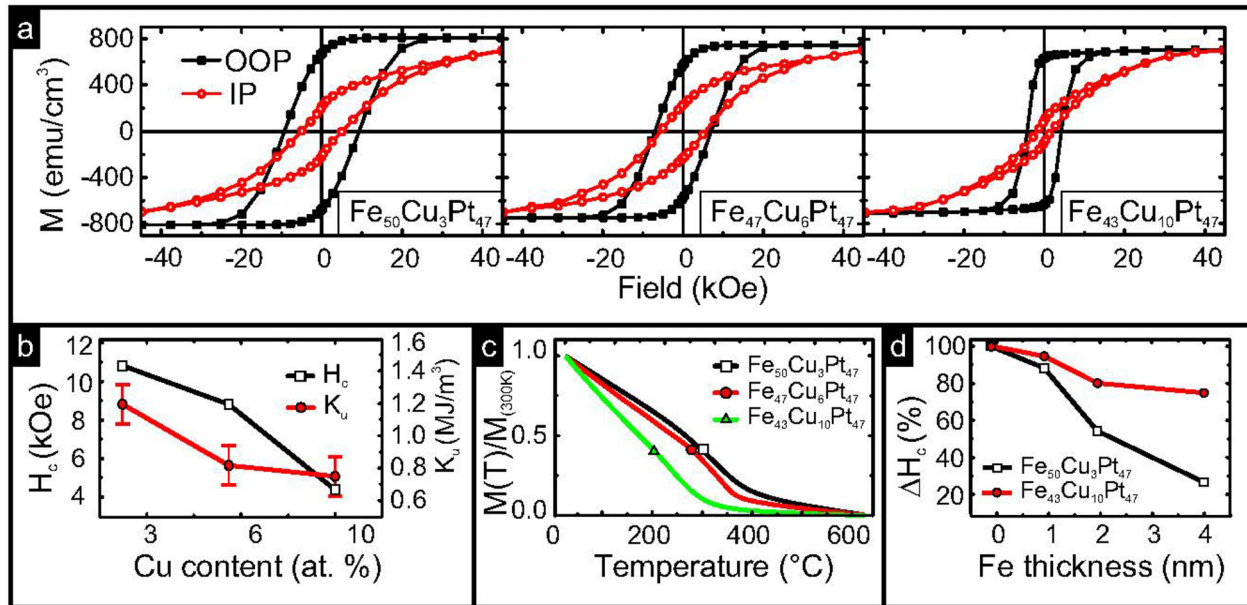


FIG. 4. (Color online) (a) SQUID M-H loops of FeCuPt thin films taken at room temperature for in-plane (IP) and out-of plane (OOP) geometry. (b) Variation of H_c and K_u as function of Cu content. (c) M-T curves of various FeCuPt films. (d) Relative change in H_c as function of Fe thickness for FeCuPt/Fe(x) bilayers at room temperature.

strong reduction in coercivity is obtained with increasing Fe layer thickness. Note that the inclusion of an in-plane oriented soft magnetic layer with a thickness larger than 2 nm will certainly limit the useful range of these structures, as any randomly oriented in-plane component will lead to noise in the read-back signal during recording.

C. FePt microstructure

The high magnetic anisotropy of the FePt L₁₀ phase in principle allows very small thermally stable grains. However,

due to the required high sputter deposition temperature, it is quite challenging to achieve such $\langle D \rangle \sim 4\text{--}5$ nm grains, which continues to be an important step toward areal density growth.

Figure 5 illustrates the microstructure of highly chemically ordered laminated triple-layered L₁₀ FePtX-Y HAMR media with a total thickness of 12 nm.⁷⁹ These particular HAMR media are FePt-C + BN/FePt-C/FePt-C + BN trilayers. The Y-segregant volume fraction is $\sim 32\%$ in each layer. The average diameter of chemically isolated grains is $\langle D \rangle = 8.4$ nm, and the size diameter distribution is $\sigma_D/\langle D \rangle = 18\%$. This is illustrated in the plane-view TEM image in

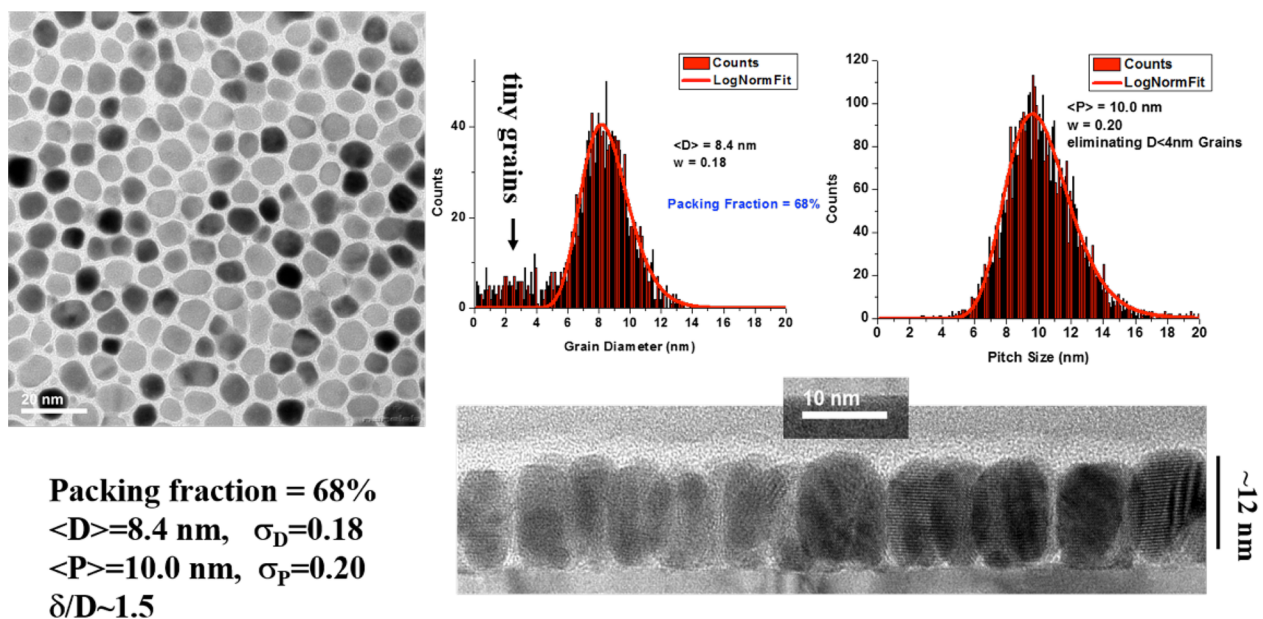


FIG. 5. (Color online) (upper left) Plan-view TEM image showing granular $\delta \sim 12$ nm thick FePtX-Y media as described in the text (upper right) grain diameter and grain pitch distributions and (bottom right) X-sectional TEM.

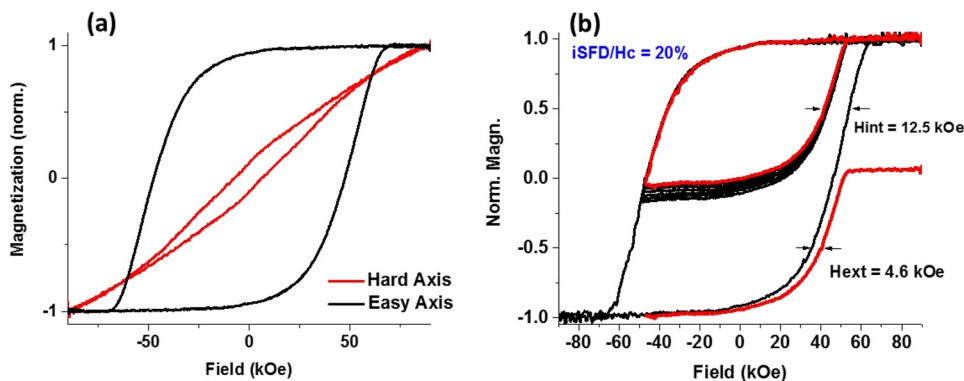


Fig. 6. (Color online) (a) In-plane and out-of-plane 9 T PPMS hysteresis measurements of FePtX-Y media, (b) major and minor loops of the same media.

Fig. 5 (top-left). Grain size and pitch distributions are highlighted in Fig. 5 (top-right), and X-sectional TEM results are shown in Fig. 5 (bottom-right).

The lateral grain structure shows well-isolated grains. These media do not suffer from grain agglomeration or the formation of elongated and laterally connected grains as is typical in single layer, e.g., FePt-C media, as highlighted in the patent reference,⁷⁹ where also quadruple laminated media are discussed. Using a pure ~ 35 vol. % C segregant in the middle layer is advantageous, as it promotes a more columnar grain shape.

Even though the segregant amount is $>30\%$, the presence of “tiny grains” with grain diameters below 3 nm is significantly reduced compared to earlier FePt media reports.^{2,15,27} We ignore tiny grains since they do not affect the distribution of grain pitch spacing in Fig. 5(b). In general, the formation of tiny grains is governed by inherent properties of the segregant to FePt interface, which also influences the grain shape. The presence of “tiny” spherical FePt grains can be avoided by limiting the “single” initial FePtX-C layer thickness to about $\delta = 2\text{--}3$ nm and adding layers, i.e., moving to (FePtX-Y) \times N multiple layer growth ($N = 2\text{--}6$). This way the total FePt thickness has almost doubled from earlier reports

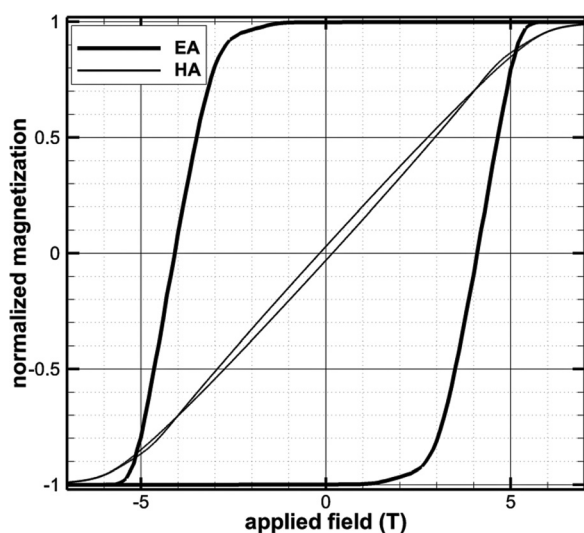


Fig. 7. EA and HA loops at 190 Oe/s sweep rate and 300 K for developmental of HAMR media.

$\langle \delta \rangle \sim 7$ nm (Refs. 24 and 27) to $\langle \delta \rangle \sim 12$ nm.² Also, the thickness–diameter ratio $\delta/D = 1.5$ is higher than earlier reported and very close to the suggested range of 1.5–2.5.^{18,19}

D. FePt magnetic properties

Normalized magnetization loops of the granular $L1_0$ -ordered FePt media described above are shown in Fig. 6. With the current experimental setup, the hard axis (HA) loops do not saturate at fields up to 9 T, indicating a high degree of ordering of FePt. High coercivity (H_C) of 4.7 T obtained from the easy axis loop also suggests the presence of highly chemically ordered and thermally stable grains in the media layer. However, the nonzero magnetic moments at zero field in the hard axis loop indicate that a certain fraction of the grains are misaligned relative to the perpendicular easy axis direction.⁸ Random texture and in-plane grains (with c-axes along the film plane) contribute to this opening. In addition, lattice mismatch in MgO/FePt interfaces and defects in texturing of the MgO seed layer cause grain misalignments. One of the improvements achieved in the current media design is the reduction of small superparamagnetic grains,²⁴ evident in the form of absence of zero field magnetization kinks in both easy and hard axis loops. A grain diameter analysis as shown in Fig. 5(b) also confirms this significant reduction in small grains. Overall, a relatively high remanent magnetization level $M_R = 94\%$ is obtained from the hysteresis loop analysis. Thermally stable grains are therefore able to maintain their orientation even at fields as low as 1 T ($M_R = 90\%$).

The effects of grain size distribution, degree of chemical ordering variations, and distributions in magnetocrystalline anisotropy have been investigated by studying easy axis reversal loops.^{2,26} An intrinsic switching field distribution (iSFD/ H_C) of 20% is obtained along with extrinsic or magnetostatic (H_{ext}) loop shifts of 4.6 kOe. This reveals noticeable improvements in the distribution of the intrinsic grain parameters, predominantly due to higher anisotropy and tighter grain size distributions. It is well known that such reduced grain size- and volume distributions lower variations of chemical ordering, H_K and K_U . Also, the columnar grain shape improves the height–diameter aspect ratio to $\delta/D \sim 1.5$.

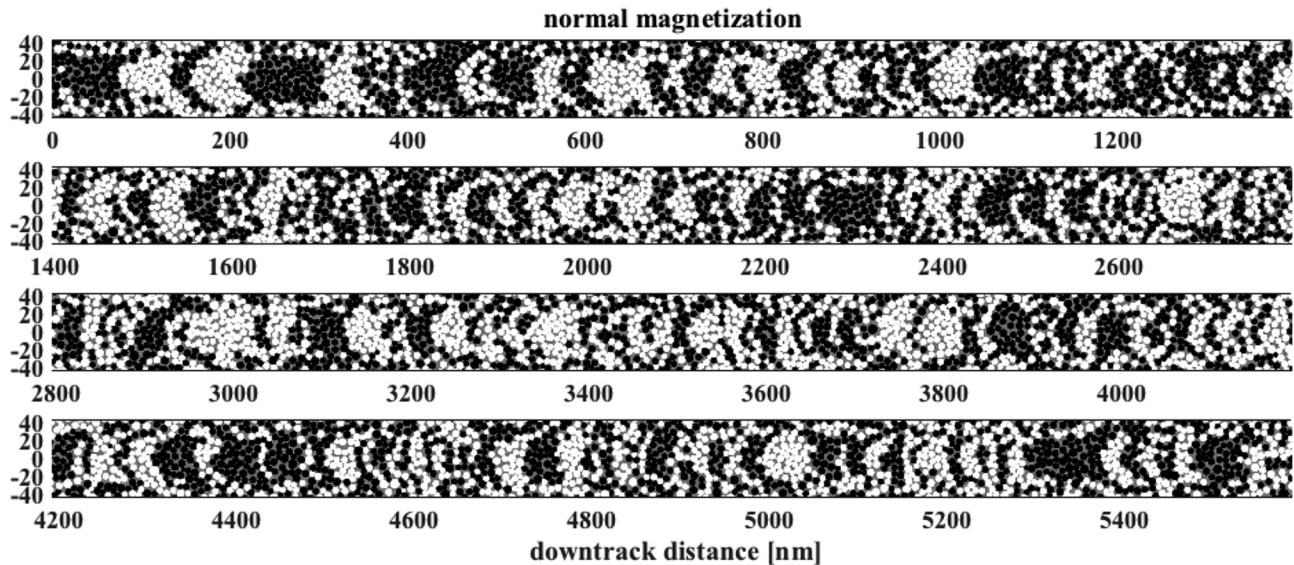


Fig. 8. Simulated track recording of a 550 bit (~ 5.6 nm) sequence using developmental HAMR media and recording head for a given hard layer realization. Each FePt grain's macrospin is down (black) or up (white). The continuous track is segmented (into four) here for viewing.

Further improvements of grain diameter- and size distributions are essential requirements for higher HAMR ADs.

IV. MODELING

Micromagnetic simulations of the recording process for HAMR systems are now capable of successfully calculating the final system performance. We demonstrate for a current experimental HAMR system at 1.3 Tb/in.². We start with a 10 nm thick recording layer, 75% packing fraction of FePt grains, and a mean center-to-center distance of $8.5 \text{ nm} \pm 18\%$. The uniaxial magnetocrystalline EA of each grain is nominally normal to the recording layer with a rocking curve width of $\sim 5^\circ$, with no in-plane or random orientations. The mean magnitude at zero temperature is $\sim 7.3 \text{ T} \pm 7\%$ with a slightly asymmetric distribution toward lower values. The normalized temperature dependence is given by a simple power law, $H_K(T)/H_K(0) = (1 - T/T_C)^\nu$ with $\nu = 0.3564$. The Curie temperature follows the usual grain size dependence in addition to an independent 2.5% Gaussian distribution around the mean value of $T_C = 694 \text{ K}$. The simulated

magnetic loops (Fig. 7) at a sweep rate of 190 Oe/s and 300 K via “kinetic micromagnetics”⁸⁰ agree well with the typical current experimental HAMR media data, discussed in Sec. III.

As standard solution of Maxwell's equations give rise to a Joule heating profile for the experimental HAMR recording head and media combination. Solution of steady-state temperature profile everywhere in the media with this source term resulted in a temperature profile in the recording layer with a peak down (cross) track gradient of 11 K/nm (12 K/nm) and a peak temperature of $\sim 850 \text{ K}$, assuming an ambient temperature 318 K and uniform motion of the head. The magnetic write field is cross track invariant with the magnitude of $\sim 1 \text{ T}$ at an angle from normal in the range of $45^\circ - 60^\circ$. Each grain's magnetic state is assumed to be described by a single macrospin whose dynamics, including magnitude, is given by Tzoufras.⁸¹

Both the applied temperature and write fields are volume averaged for each media grain. For the given read sensor geometry, the reader response is computed, and reciprocity

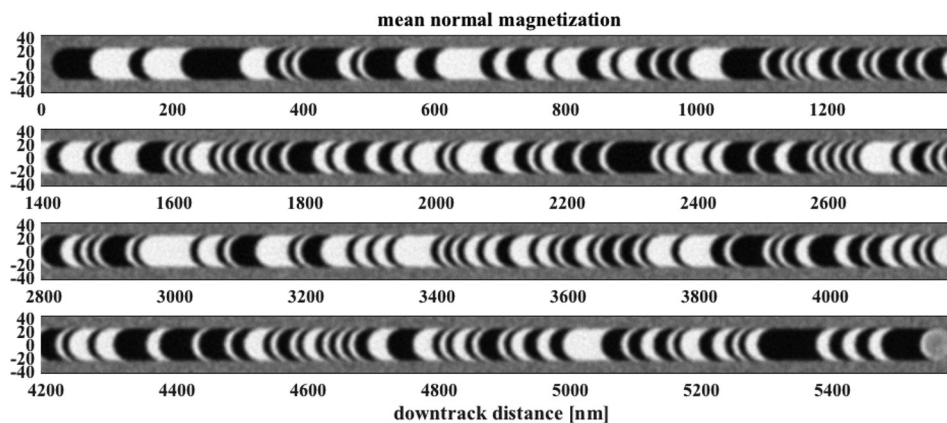


Fig. 9. Same as Fig. 8 except mean magnetization over the 400 media realizations.

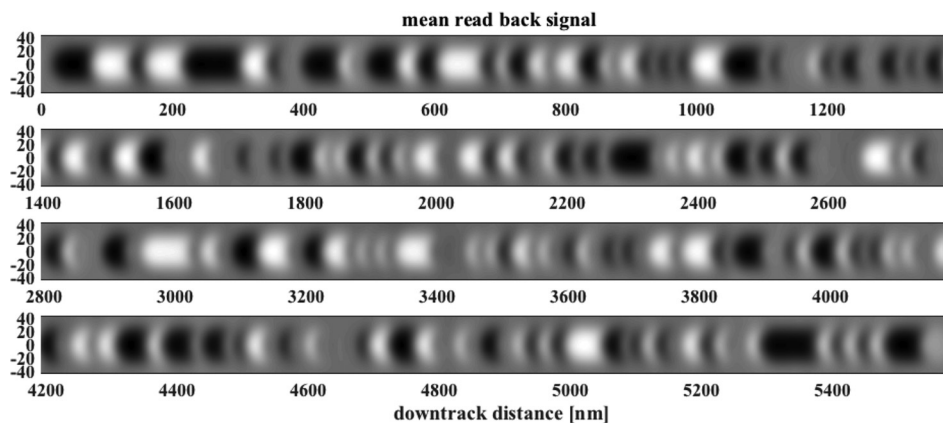


FIG. 10. Same as Fig. 9 except mean read back signal.

is assumed to calculate the read back signal with a small Gaussian noise added to mimic the sensor noise.

As in experiment, we record repeats of a 511-bit pseudo-random bit sequence (PRBS). Each repeat (400 here) is simulated on a different hard layer realization. By simulating slightly longer 550 bit-sequence recording that includes a synchronization mark, these repeats are then stitched together (Figs. 8 and 9). The computational wall time for one 550 bit-sequence simulation depends on the linear velocity and maximum linear density desired. On a modern workstation, using a single central processing unit thread, ~ 3 h was required for the simulations reported here. We note that the repeats can be run on parallel threads, since they are independent. The resulting read back signal (Figs. 10 and 11) is then input to a developmental channel model giving the predicted HAMR system performance in terms of a BER. For an acceptable on-track BER ($< 10^{-2}$), the simulated system was able to achieve 598 ktpi and 2510 kfc/i in accordance with experimental results.

In summary, simulations are now accurate and fast enough to allow for prediction of HAMR AD capability as demonstrated with this experimental 1.3 Tb/in.² system. It is

also now possible to simulate ~ 275 000 bits allowing for direct comparison between simulation and experimental data. Furthermore, simulations can correctly identify the limiting factors for HAMR AD, allowing for more focused and faster development toward a commercial HAMR HDD.

V. SUMMARY AND OVERVIEW

Noise performance and spatial resolution are key parameters in recording media and are ongoing challenges in advancing the areal density of hard disk drive technology. The dominant media noise source today is transition jitter. In sputtered media, it reflects the finite size, random positioning, and dispersions in size, orientation, and magnetic properties of the fine grains that comprise the media. Highly anisotropic materials, combined with heat-assisted magnetic recording, promise significant reductions in the average, thermally stable grain size from currently about 7–9 nm in perpendicular magnetic recording CoCrPt-alloys down to about 4–5 nm in chemically ordered L₁₀ FePt-based HAMR media. HAMR limitations and extendibility are studied in light of the recent Seagate 1–1.4 Tb/in.² technology

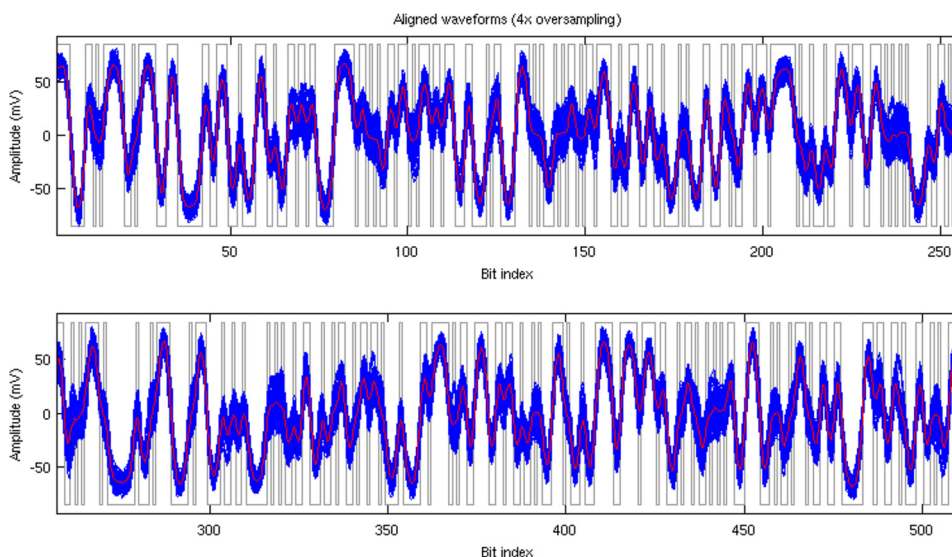


FIG. 11. (Color online) All 400 realization (blue) and mean (red) of on-track read back signal of simulated 511 PRBS.

demonstrations,^{3–5} modeling of which is discussed in Sec. IV. Besides magnetic field component dependence on magnetic media properties, thermal spot size and media temperature rise strongly dependent on the media thermal conductivity. Media are optimized by growing granular L1₀ FePt films on a relatively thin, e.g., MgO, seed layer which is on top of a thicker thermal conductor or heat sink layer. The achievable areal density depends on the near field transducer dimension and the media thermal properties. The main conclusions are that besides grain size, shape, and distribution requirements, the thermal properties of both magnetic and seed layers need to be improved and optimized to achieve the required SNR for higher areal densities. The current HAMR Media Technology Roadmap is discussed by the industry at the Advanced Storage Technology Center (ASTC) to reach a HAMR areal density of 4 Tb/in.² or beyond.²³ Future modeling efforts, as highlighted in the HAMR media overview in Sec. II, predict significant enhancements of AD up to 20 Tb/in.² and beyond when using ECC-type bilayer FePt/Fe media.⁶⁶

ACKNOWLEDGMENTS

The authors thank the Advanced Storage Technology Consortium (ASTC) for discussions and suggestions. D.W., O.M., and G.P. thank the former HGST HAMR media team for their support. D.M. and N.S. thank Mattias Wachs for help in FeCuPt sample preparation.

- ¹D. Weller and A. Moser, *IEEE Trans. Magn.* **35**, 4423 (1999).
- ²D. Weller, O. Mosendz, G. Parker, S. Pisana, and T. S. Santos, *Phys. Status Solidi A* **210**, 1245 (2013).
- ³A. Q. Wu *et al.*, *IEEE Trans. Magn.* **49**, 779 (2013).
- ⁴X. Wang, K. Gao, H. Zhou, A. Itagi, M. Seigler, and E. Gage, *IEEE Trans. Magn.* **49**, 686 (2013).
- ⁵G. Ju *et al.*, *IEEE Trans. Magn.* **51**, 3201709 (2015).
- ⁶R. W. Wood and D. A. Peterson, *IEEE Trans. Commun.* **34**, 454 (1986).
- ⁷R. Radhakrishnan, B. Vasić, F. Erden, and C. He, “Characterization of heat-assisted magnetic recording channels,” in *DIMACS Series in Discrete Mathematics and Theoretical Computer Science* (2007), Vol. 73.
- ⁸S. Wicht *et al.*, *J. Appl. Phys.* **117**, 013907 (2015).
- ⁹S. Wicht, S. H. Wee, O. Hellwig, V. Mehta, S. Jain, D. Weller, and B. Rellinghaus, *J. Appl. Phys.* **119**, 115301 (2016).
- ¹⁰W. A. Challener *et al.*, *Nat. Photonics* **3**, 220 (2009).
- ¹¹L. Shi *et al.*, *Nanoscale Microscale Thermophys. Eng.* **19**, 127 (2015).
- ¹²F. Everaardt, *WD Executive Summit: Trends in Data Storage, From SSD to HAMR and Shingle/PMR* (2013).
- ¹³R. E. Rottmayer *et al.*, *IEEE Trans. Magn.* **42**, 2417 (2006).
- ¹⁴S. D. Granz and M. H. Kryder, *J. Magn. Magn. Mater.* **324**, 287 (2012).
- ¹⁵K. Hono and Y. K. Takahashi, “L1₀-FePt granular films for heat-assisted magnetic recording media,” in *Ultra-High-Density Magnetic Recording, Storage Materials and Media Designs*, edited by G. Varvaro and F. Casoli (Pan Stanford, 2016), Chap. 5, pp. 245–277.
- ¹⁶C.-B. Rong, D. Li, V. Nandwana, N. Poudyal, Y. Ding, Z. L. Wang, H. Zeng, and J. P. Liu, *Adv. Mater.* **18**, 2984 (2006).
- ¹⁷H. M. Lu, Z. H. Cao, C. L. Zhao, P. Y. Li, and X. K. Meng, *J. Appl. Phys.* **103**, 123526 (2008).
- ¹⁸A. Lyberatos, D. Weller, and G. Parker, *J. Appl. Phys.* **112**, 113915 (2012).
- ¹⁹A. Lyberatos, D. Weller, and G. Parker, *J. Appl. Phys.* **114**, 233904 (2013).
- ²⁰O. Hovorka, S. Devos, Q. Coopman, W. J. Fan, C. J. Aas, R. F. L. Evans, X. Chen, G. Ju, and R. W. Chantrell, *Appl. Phys. Lett.* **101**, 052406 (2012).
- ²¹A. Kussmann and G. von Rittberg, *Ann. der Phys.* **442**, 173 (1950).
- ²²J. Lyubina, B. Rellinghaus, O. Gutfleisch, and M. Albrecht, “Structure and magnetic properties of L1₀-ordered Fe–Pt alloys and nanoparticles,” in *Handbook of Magnetic Materials*, edited by K. H. J. Buschow (Elsevier, 2011), Chap. 5.
- ²³D. Weller, G. Parker, O. Mosendz, E. Champion, B. Stipe, X. Wang, T. Klemmer, G. Ju, and A. Ajan, *IEEE Trans. Magn.* **50**, 3100108 (2014).
- ²⁴O. Mosendz, S. Pisana, J. W. Reiner, B. Stipe, and D. Weller, *J. Appl. Phys.* **111**, 07B729 (2012).
- ²⁵L. Zhang, Y. K. Takahashi, K. Hono, B. C. Stipe, J. Y. Juang, and M. Grobis, *IEEE Trans. Magn.* **47**, 4062 (2011).
- ²⁶S. Pisana, O. Mosendz, G. J. Parker, J. W. Reiner, T. S. Santos, A. T. McCallum, H. J. Richter, and D. Weller, *J. Appl. Phys.* **113**, 043910 (2013).
- ²⁷B. H. D. Ch. S. Varaprasad, M. Chen, Y. K. Takahashi, and K. Hono, *IEEE Trans. Magn.* **49**, 718 (2013).
- ²⁸S. Wicht, V. Neu, L. Schultz, B. Rellinghaus, D. Weller, O. Mosendz, G. Parker, and S. Pisana, *J. Appl. Phys.* **114**, 063906 (2013).
- ²⁹J. Becker, O. Mosendz, D. Weller, A. Kirilyuk, J. C. Maan, P. C. M. M. Christianon, Th. Rasing, and A. Kimel, *Appl. Phys. Lett.* **104**, 152412 (2014).
- ³⁰J.-G. Zhu and H. Li, *IEEE Trans. Magn.* **49**, 3568 (2013).
- ³¹R. H. Victora and P.-W. Huang, *IEEE Trans. Magn.* **49**, 751 (2013).
- ³²F. Scheibel, F. Haering, P. Ziemann, and U. Wiedwald, *J. Phys. D: Appl. Phys.* **48**, 085001 (2015).
- ³³D. A. Gilbert, L. W. Wang, T. J. Klemmer, J. U. Thiele, C. H. Lai, and K. Liu, *Appl. Phys. Lett.* **102**, 132406 (2013).
- ³⁴D. A. Gilbert, J.-W. Liao, L.-W. Wang, J. W. Lau, T. J. Klemmer, J.-U. Thiele, C.-H. Lai, and K. Liu, *APL Mater.* **2**, 086106 (2014).
- ³⁵D. Chernyshov, T. Treves, C. Le, H. Pappasoi, A. Yuan, R. Ajan, and R. Aharya, *IEEE Trans. Magn.* **49**, 3572 (2013).
- ³⁶C. Brombacher, M. Grobis, J. Lee, J. Fidler, T. Eriksson, T. Werner, O. Hellwig, and M. Albrecht, *Nanotechnology* **23**, 025301 (2012).
- ³⁷M. L. Yan, Y. F. Xu, and D. J. Sellmyer, *J. Appl. Phys.* **99**, 08G903 (2006).
- ³⁸T. Maeda, A. Kikitsu, T. Kai, T. Nagase, H. Aikawa, and J. Akiyama, *IEEE Trans. Magn.* **38**, 2796 (2002).
- ³⁹M. Albrecht and C. Brombacher, *Phys. Status Solidi* **210**, 1272 (2013).
- ⁴⁰M. Maret, C. Brombacher, P. Matthes, D. Makarov, N. Boudet, and M. Albrecht, *Phys. Rev. B* **86**, 024204 (2012).
- ⁴¹S. Laureti, C. Brombacher, D. Makarov, M. Albrecht, D. Peddis, G. Varvaro, and F. D’Acapito, *J. Appl. Crystallogr.* **47**, 1722 (2014).
- ⁴²J. Wang, S. Hata, Y. K. Takahashi, H. Sepehri-Amin, B. H. D. Ch. S. Varaprasad, T. Shiroyama, T. Schrefl, and K. Hono, *Acta Mater.* **91**, 41 (2015).
- ⁴³H.-J. Richter, G. Parker, M. Staffaroni, and B. Stipe, *IEEE Trans. Magn.* **49**, 5378 (2013).
- ⁴⁴Y. Ikeda, M. E. Schabes, Y. Sonobe, K. Takano, and D. Weller, “Magnetic recording disk with composite perpendicular recording layer,” U.S. patent 6,468,670 (22 October 2002).
- ⁴⁵R. H. Victora and X. Shen, *IEEE Trans. Magn.* **41**, 2828 (2005).
- ⁴⁶D. Suess, *Appl. Phys. Lett.* **89**, 113105 (2006).
- ⁴⁷D. Suess, J. Lee, J. Fidler, and T. Schrefl, *J. Magn. Magn. Mater.* **321**, 545 (2009).
- ⁴⁸J. Wang, H. Sepehri-Amin, Y. K. Takahashi, S. Okamoto, S. Kasai, J. Y. Kim, T. Schrefl, and K. Hono, *Acta Mater.* **111**, 47 (2016).
- ⁴⁹J.-U. Thiele, K. R. Coffey, M. F. Toney, J. A. Hedstrom, and A. J. Kellock, *J. Appl. Phys.* **91**, 6595 (2002).
- ⁵⁰J.-U. Thiele, S. Maat, and E. E. Fullerton, *Appl. Phys. Lett.* **82**, 2859 (2003).
- ⁵¹D. A. Gilbert, J.-W. Liao, B. J. Kirby, M. Winklhofer, G. T. Zimanyi, C.-H. Lai, and K. Liu, *Sci. Rep.* **6**, 32842 (2016).
- ⁵²Z. Liu, Y. Jiao, and R. H. Victora, *Appl. Phys. Lett.* **108**, 232402 (2016).
- ⁵³D. Suess, T. Schrefl, S. Fühler, M. Kirschner, G. Hrkac, F. Dorfbauer, and J. Fidler, *Appl. Phys. Lett.* **87**, 012504 (2005).
- ⁵⁴R. H. Victora and X. Shen, *IEEE Trans. Magn.* **41**, 537 (2005).
- ⁵⁵D. Goll, A. Breitling, and S. Macke, *IEEE Trans. Magn.* **44**, 3472 (2008).
- ⁵⁶F. Casoli, F. Albertini, L. Nasi, S. Fabbri, R. Cabassi, F. Bolzoni, and C. Bocchi, *Appl. Phys. Lett.* **92**, 142506 (2008).
- ⁵⁷L. S. Huang, J. F. Hu, and J. S. Chen, *J. Magn. Magn. Mater.* **324**, 1242 (2012).
- ⁵⁸J.-L. Tsai, H.-T. Tzeng, and G.-B. Lin, *J. Nanomater.* **2012**, 129097.
- ⁵⁹D. Goll, A. Breitling, L. Gu, P. A. van Aken, and W. Sigle, *J. Appl. Phys.* **104**, 083903 (2008).
- ⁶⁰D. Goll and A. Breitling, *Appl. Phys. Lett.* **94**, 052502 (2009).

- ⁶¹L. Liu, W. Sheng, J. Bai, J. Cao, Y. Lou, Y. Wang, F. Wei, and J. Lu, *Appl. Surf. Sci.* **258**, 8124 (2012).
- ⁶²W. Tipcharoen, A. Kaewrawang, and A. Siritaratiwat, *Adv. Mater. Sci. Eng.* **2015**, 504628.
- ⁶³A. T. McCallum, P. Krone, F. Springer, C. Brombacher, M. Albrecht, E. Dobisz, M. Grobis, D. Weller, and O. Hellwig, *Appl. Phys. Lett.* **98**, 242503 (2011).
- ⁶⁴J. Lee, D. Makarov, C. Brombacher, B. Dymerska, D. Suess, M. Albrecht, and J. Fidler, *Nanotechnology* **25**, 045604 (2014).
- ⁶⁵D. Makarov, J. Lee, C. Brombacher, C. Schubert, M. Fuger, D. Suess, J. Fidler, and M. Albrecht, *Appl. Phys. Lett.* **96**, 062501 (2010).
- ⁶⁶D. Suess and T. Schrefl, *Appl. Phys. Lett.* **102**, 162405 (2013).
- ⁶⁷H. J. Richter, A. Lyberatos, U. Nowak, R. F. L. Evans, and R. W. Chantrell, *J. Appl. Phys.* **111**, 033909 (2012).
- ⁶⁸C. Brombacher, H. Schletter, M. Daniel, P. Matthes, N. Jöhrmann, M. Maret, D. Makarov, M. Hietschold, and M. Albrecht, *J. Appl. Phys.* **112**, 073912 (2012).
- ⁶⁹G. S. Abo, Y.-K. Hong, J. Park, J. Lee, W. Lee, and B.-C. Choi, *IEEE Trans. Magn.* **49**, 4937 (2013).
- ⁷⁰“Hoya,” <http://www.hoyaoptics.com/pdf/OpticalGlass.pdf>.
- ⁷¹“Ohara,” <http://www.oharacorp.com/pdf/TS-10.pdf>.
- ⁷²“Asahi,” http://www.agc.com/english/products/products_02_02.html#a04.
- ⁷³B. H. D. Ch. S. Varaprasad, A. Ajan, and K. Hono, *J. Appl. Phys.* **113**, 203907 (2013).
- ⁷⁴S. D. Granz, K. Barmak, and M. H. Kryder, *Eur. Phys. J. B* **86**, 81 (2013).
- ⁷⁵J. A. Christodoulides, P. Farber, M. Daniil, H. Okumura, G. C. Hadjipanayis, V. Skumryev, A. Simopoulos, and D. Weller, *IEEE Trans. Magn.* **37**, 1292 (2001).
- ⁷⁶T. Shiroyama, B. S. D. C. S. Varaprasad, Y. K. Takahashi, and K. Hono, *IEEE Trans. Magn.* **50**, 3202404 (2014).
- ⁷⁷L. Zhang, Y. K. Takahashi, A. Perumal, and K. Hono, *J. Magn. Magn. Mater.* **322**, 2658 (2010).
- ⁷⁸B. H. D. Ch. S. Varaprasad *et al.* *Appl. Phys. Lett.* **104**, 222403 (2014).
- ⁷⁹O. Hellwig, O. Mosendz, and D. K. Weller, “Layered segregant heat assisted magnetic recording (HAMR) media,” U.S. patent 20160099017 A1 (7 April 2016).
- ⁸⁰G. J. Parker and W. N. G. Hitchon, *Phys. Lett. A* **377**, 2388 (2013).
- ⁸¹M. Tzoufras, *New J. Phys.* **17**, 103014 (2015).